PHYSICAL REVIEW B **96**, 241401(R) (2017)

Spin-orbit interaction in a dual gated InAs/GaSb quantum well

Arjan J. A. Beukman,[1] Folkert K. de Vries,[1] Jasper van Veen,[1] Rafal Skolasinski,[1] Michael Wimmer,[1] Fanming Qu,[1] David T. de Vries,[1] Binh-Minh Nguyen,[2] Wei Yi,[2] Andrey A. Kiselev,[2] Marko Sokolich,[2] Michael J. Manfra,[3] Fabrizio Nichele,[4] Charles M. Marcus,[4] and Leo P. Kouwenhoven[1,5,*]

[1]*QuTech and Kavli Institute of Nanoscience, Delft University of Technology, 2600 GA Delft, The Netherlands*

[2]*HRL Laboratories, 3011 Malibu Canyon Road, Malibu, California 90265, USA*

[3]*Department of Physics and Astronomy and Microsoft Station Q Purdue, Purdue University, West Lafayette, Indiana 47907, USA*

[4]*Center for Quantum Devices, and Microsoft Station Q Copenhagen, Niels Bohr Institute, University of Copenhagen, 2100 Copenhagen, Denmark*

[5]*Microsoft Station Q Delft, 2600 GA Delft, The Netherlands*

(Received 31 March 2017; revised manuscript received 29 August 2017; published 1 December 2017)

The spin-orbit interaction is investigated in a dual gated InAs/GaSb quantum well. Using an electric field, the quantum well can be tuned between a single-carrier regime with exclusively electrons as carriers and a two-carrier regime where electrons and holes coexist. The spin-orbit interaction in both regimes manifests itself as a beating in the Shubnikov–de Haas oscillations. In the single-carrier regime the linear Dresselhaus strength is characterized by $\beta = 28.5$ meV Å and the Rashba coefficient α is tuned from 75 to 53 meV Å by changing the electric field. In the two-carrier regime a quenching of the spin splitting is observed and attributed to a crossing of spin bands.

DOI: 10.1103/PhysRevB.96.241401

The semiconductors InAs and GaSb have small band gaps together with a crystal inversion asymmetry resulting from their zinc-blende structure. These materials are therefore predicted to have a strong spin-orbit interaction (SOI) [1,2] which has been measured experimentally [3]. Moreover, tuning of the Rashba strength by electrostatic gating has been shown for InAs quantum wells [4,5]. Strong and *in situ* control over the SOI is a promising route towards novel spintronic devices [2,6,7], and a strong SOI together with a large g-factor and induced superconductivity are ingredients for a topological superconducting phase [8].

Combining InAs and GaSb in a quantum well gained much interest because of the type-II broken-gap band alignment [9]. As a result, the GaSb valence band maximum is higher in energy than the InAs conduction band minimum, opening a range of energies where electrons in the InAs coexist with holes in the GaSb. The spatial separation of these electron and hole gases allows for tunability of the band alignment using an electric field. Therefore, a rich phase diagram can be mapped out using dual gated devices [10,11]. Although spatially separated, strong coupling between the materials allows for electron-hole hybridization which opens a gap in the energy spectrum when the density of electrons equals that of holes [12,13], driving the band structure topologically nontrivial [10].

Interestingly, the magnitude of this hybridization gap is spin dependent due to the SOI [14–16]. Therefore, a spin-polarized state is seen at energies close to the hybridization gap [17], and at higher energies a dip in the spin splitting is expected [18]. The latter has yet to be observed and indicates a competition between electron-hole hybridization and the spin-orbit interaction. Here, we experimentally study SOI through the difference in density of the spin-orbit split bands of an InAs/GaSb quantum well. This zero-field density difference (Δn_{ZF}) is extracted from magnetoresistance measurements. First, the SOI is investigated in the regime where the GaSb is depleted from carriers. Rashba and Dresselhaus SOI strengths can be extracted from measurements of Δn_{ZF}. Second, SOI is investigated just above the hybridization gap where Δn_{ZF} almost vanishes, consistent with band-structure calculations.

A 20-μm-wide and 80-μm-long Hall bar device is defined using chemical wet etching techniques. A top gate is separated from the mesa by a 80-nm-thick SiN_x dielectric layer. The Hall bar is fabricated from the same wafer used in Refs. [11,19]. The quantum well consists of 12.5 nm InAs and 5 nm GaSb between 50 nm AlSb barriers. The doped GaSb substrate acts as a back gate. All measurements are done at 300 mK using standard lock-in techniques with an excitation current of 50 nA.

Figure 1 presents the longitudinal resistance of the Hall bar device as a function of top gate voltage V_{tg} and back gate voltage V_{bg}. The measurement is performed in a 2 T perpendicular magnetic field and therefore shows quantum oscillations resulting from the changing electron density. Quantum oscillations corresponding to holes are less pronounced as the mobility of holes in this system is much lower than the mobility of electrons [11]. For lines parallel to these oscillations, such as line I in Fig. 1(a), the electron density is constant while the electric field changes. Regions of high resistance, indicated by the dashed white and green lines, correspond to having the Fermi level inside an energy gap. A detailed description of the phase diagram obtained from measurements on the same wafer was reported by Qu *et al.* [11].

The green solid line in Fig. 1 divides the phase diagram into two regimes. To the right-hand side of this line is the electron-only regime, where the GaSb is depleted. The system effectively is an asymmetric InAs quantum well with a trivial band alignment and a Fermi level residing in the conduction band [see the inset of Fig. 1(a)]. In this regime we investigate Δn_{ZF} along line I, where the electron mobility is highest while only the lowest subband remains occupied. The regime to the left of the green line is the two-carrier regime where electrons

*Corresponding author: l.p.kouwenhoven@tudelft.nl

 ©2017 American Physical Society

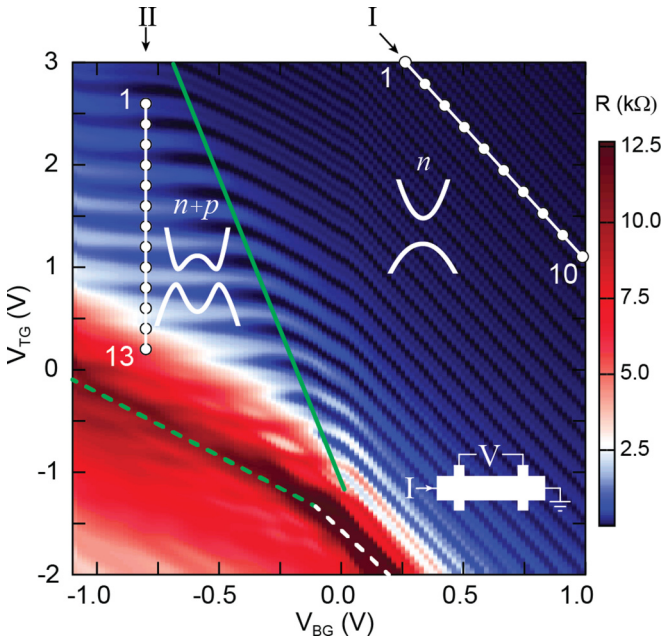

FIG. 1. Longitudinal resistance of the Hall bar device (see bottom right inset) as a function of top gate voltage (V_{tg}) and back gate voltage (V_{bg}) at 2 T out-of-plane magnetic field. Oscillations in resistance originate from Landau levels and denote lines of constant electron density. The dashed green and white lines indicate regions with the Fermi level located inside an energy gap. The solid green line separates the region with electrons as carriers (right) from a region where electrons and holes coexist (left). Line I is situated in the electron regime and line II in the two-carrier regime. The insets show the schematic band alignment for both cases.

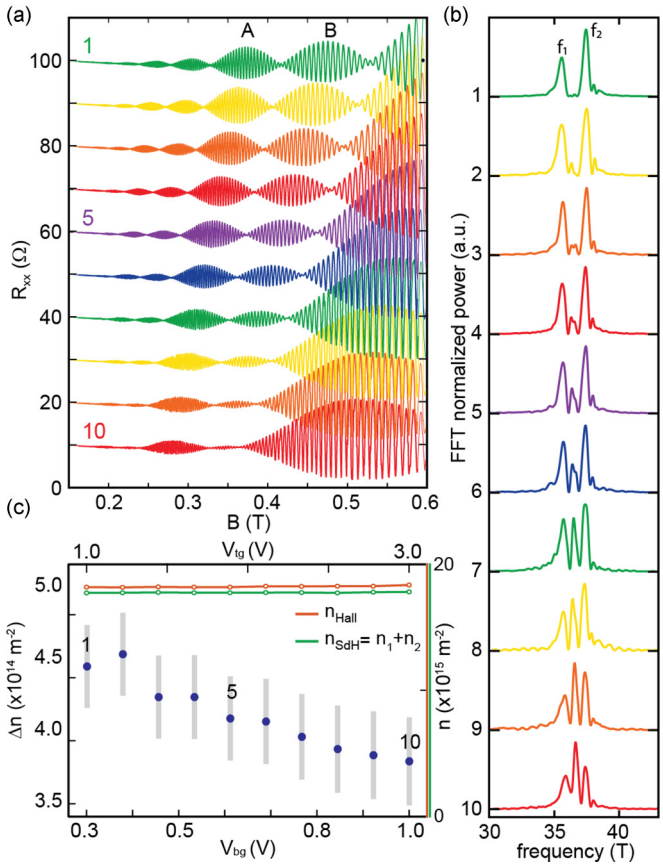

FIG. 2. Spin splitting at a constant electron density in the electron regime. (a) Magnetoresistance traces for data points 1–10 along line I indicated in Fig. 1. A constant background is subtracted from the traces and they are offset 10 Ω from each other. (b) Fourier power spectra $|\mathcal{F}[R_{xx}(1/B)]|^2$ of the traces in (a). (c) Electron density extracted from Hall resistance and Shubnikov–de Haas period (right axis) together with the Δn_{ZF} at each data point along line I (left axis), with error bars in gray.

and holes coexist. Line II is chosen to evaluate Δn_{ZF} close to the hybridization gap (highlighted by the dashed green line). Before discussing the spin-orbit interaction in the two-carrier regime (along line II) we first study the electron-only regime (line I).

Figure 2(a) shows magnetoresistance traces for ten points along line I. The density of electrons is fixed [see Fig. 2(c)] while the electric field is changed. We first consider trace 1. Clear oscillations in the longitudinal resistance R_{xx} are observed as a function of perpendicular magnetic field B modulated by a beat pattern. These Shubnikov–de Haas (SdH) oscillations appear for each single spin band and are periodic in $1/B$ with a frequency that relates to the carrier density via $n = e/h \cdot f$ [3,20]. The beat modulation observed in trace 1 is caused by two slightly different SdH frequencies f_1, f_2. This is also evident from the fast Fourier transform (FFT) of the magnetoresistance trace $\mathcal{F}[R_{xx}(1/B)]$ presented in the first curve of Fig. 2(b) (see the Supplemental Material for details on the Fourier procedure [21]). These two SdH frequencies indicate two distinct densities n_1,n_2. They must correspond to different spin species because their sum $n_1 + n_2$ equals the Hall density n_H [see Fig. 2(c)]. Subsequently, one spin species has a larger density than the other, $n_1 > n_2$, implying that the system favors one spin-orbit eigenstate over to the other. The difference, $\Delta n_{ZF} = n_2 - n_1$, is a measure for the zero-field spin-splitting energy, $\Delta E_{ZFSS} = \Delta n_{ZF}(m^*/\pi\hbar^2)^{-1}$.

Upon moving from point 1 to 10 along line I, two trends are observed. First, an extra frequency peak emerges in the FFTs at $(f_1 + f_2)/2$. This originates from the asymmetry between adjacent beats in the SdH oscillations, visible both in the amplitude and number of oscillations of beats A and B in Fig. 2(a) [21]. Second, the spacing between the outer peaks in the FFT spectrum decreases, as is evident from the decreasing Δn_{ZF} over line I [Fig. 2(c)]. This arises from an increasing number of oscillations in both beats A and B (see Ref. [21]), which also pushes the beat nodes to lower magnetic fields. Before we extract the actual SOI strengths and show its electric field dependence, we first elucidate the origin of the emerging center frequency peak.

The center frequency, interestingly, does not correspond to an actual density. The sum of the densities n_1 and n_2 (corresponding to the outer peaks in the FFT) still equals the Hall density. There are, however, mechanisms involving scattering between Fermi surfaces that can result in extra frequency components. Such mechanisms are magnetic intersubband scattering (MIS) [22,23], magnetophonon resonances (MPRs) [24,25], and magnetic breakdown (MB) [26–28].

We exclude MIS and MPR. By changing the electron density all the frequency peak positions shift with equal strength [21]. However, the oscillation frequency of MIS and MPR is determined by the subband spacing and a specific phonon frequency, respectively. Both do not depend on the electron density. In contrast, for MB the spurious peak always appears in between f_1 and f_2. The MB mechanism explains this spurious central peak as carriers tunneling between spin-polarized Fermi surfaces at spin-degeneracy points. The interplay of Dresselhaus and Rashba SOIs in our heterostructure could lead to such an anisotropic Fermi surface [26,29]. As the ratio of Rashba and Dresselhaus SOI strengths approaches 1, the magnetic breakdown is enhanced and a central peak is expected [26]. In order to confirm this hypothesis, we extract the individual Rashba and Dresselhaus contributions by comparing our data to quantum mechanical Landau level simulations that include the MB mechanism.

The quantum well in this electron-only regime is modeled by a Hamiltonian with a spin-orbit interaction in two-dimensional (2D) electron systems subject to a perpendicular magnetic field B, as given by [1,2]

$$H = \frac{\left(\hat{p}_x^2+\hat{p}_y^2\right)}{2m^*}\sigma_0+\alpha(\hat{p}_y\sigma_x - \hat{p}_x\sigma_y)/\hbar+\beta(\hat{p}_x\sigma_x - \hat{p}_y\sigma_y)/\hbar + \gamma(\hat{p}_y\hat{p}_x\hat{p}_y\sigma_x - \hat{p}_x\hat{p}_y\hat{p}_x\sigma_y)/\hbar^3 + \frac{1}{2}g\mu_B B\sigma_z, \quad (1)$$

where $p_i \rightarrow p_i + eA_i$ is the canonical momentum, σ_i Pauli spin matrices, α,β,γ the Rashba, linear Dresselhaus, and cubic Dresselhaus coefficients, respectively, $\hbar$ the reduced Planck's constant, and μ_B the Bohr magneton. An electron effective mass of $m^* = 0.04m_0$ is measured from the temperature dependence of the SdH oscillations [21] and a g-factor of -11.5 is used in the calculations [30,31]. We solve for the Landau level energies in a perpendicular magnetic field B_z and extract the resistivity as a function of magnetic field (see the Supplemental Material for details [21]).

The parameters α,β,γ in the model are estimated and fine tuned to match the node positions and the number of oscillations in a beat of the measured SdH traces. Figures 3(a) and 3(b) show the measured SdH data together with the simulated data for traces 1 and 10. Trace 1 is fitted with $\alpha_1 = 75$ meV Å, $\beta_1 = 28.5$ meV Å, $\gamma_1 = 0$ meV Å^3, and trace 10 is fitted with $\alpha_{10} = 53$ meV Å, $\beta_{10} = 28.5$ meV Å, $\gamma_{10} = 0$ meV Å^3. The node positions and amplitude modulation of the simulated data agree well with the measured SdH oscillations.

Curiously, only good fits are obtained when setting the cubic Dresselhaus term γ to zero. In 2D systems, β is related to γ via $\beta = \langle k_z^2\rangle\gamma$, where $\langle k_z^2\rangle \approx (\pi/d)^2$ is the expectation value of the transverse momentum [1,2] in a quantum well of thickness d. So γ should be nonzero. Currently we do not understand this discrepancy. A recent experimental study on a similar material system also found that the cubic Dresselhaus term could be neglected [32].

Now we consider all traces (1–10) and show that the two trends of Fig. 2 (emerging center FFT peak and approaching outer FFT peaks) are reproduced by changing only the Rashba SOI strength. Figure 3(c) shows the FFTs of the simulated

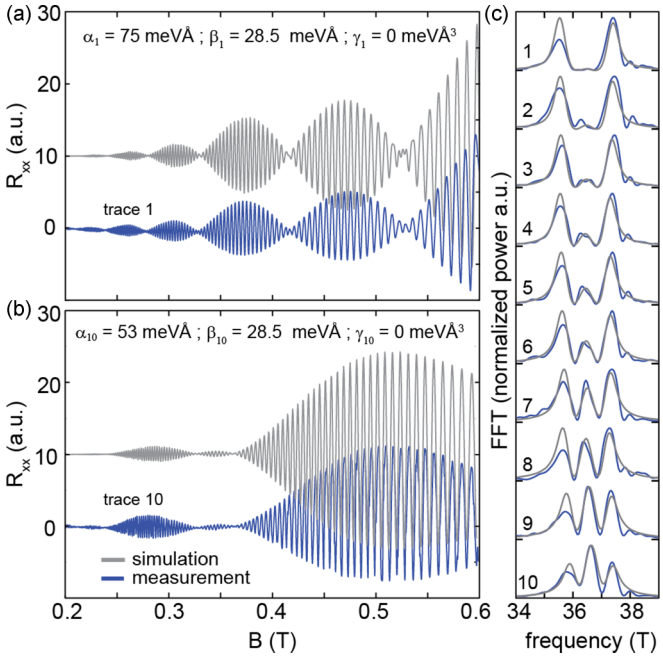

FIG. 3. Landau level simulations for a 2DEG with Rashba and Dresselhaus spin-orbit interactions. (a) and (b) depict the measured trace (blue) together with the simulated magnetoresistance trace (gray) which is offset by ten units. The values for α, β, and γ used are mentioned in the figure. In all the simulations the Landau level broadening is set to $\Gamma = 0.45$ meV. (c) Fast Fourier transform of the simulated and measured magnetoresistance at points 1–10 along line I. All simulated magnetoresistance traces can be found in the Supplemental Material [21].

traces where α is linearly interpolated between α_1 and α_{10} while fixing $\beta = 28.5$ meV Å and $\gamma = 0$ meV Å^3. Linear interpolation is used because the electric field changes linearly along line I, and the Rashba SOI strength depends linearly on electric field [1,33,34]. All simulated FFTs and the SdH traces [21] match the measured data very well, clearly reproducing the emerging central peak and the approaching outer peaks.

In the remainder of this Rapid Communication we switch to the two-carrier regime, located to the left of the solid green line in Fig. 1. Electrons in InAs are present alongside the holes in GaSb ($n + p$). Here, we study the influence of the hybridization of electrons with holes on Δn_{ZF} by investigating magnetoresistance traces on points 1–13 along line II.

Before continuing with the measured magnetoresistance traces, it is insightful to examine the expected band structures at points 1 and 13, as illustrated in Fig. 4(b). The first point of line II is located near the boundary between the two-carrier and single-carrier regimes. A small amount of holes with a large amount of electrons is present. At point 13, close to the hybridization gap, the electron and hole densities are roughly equal, hence the Fermi level E_f is close to the hybridization gap. Note also that k_{cross} decreases from 1 to 13, since the electric field changes.

Figure 4(a) shows the magnetoresistance traces 1–13 along line II. Starting from trace 1 towards trace 13 we find a series of traces with or without beating, depicted in blue and red,

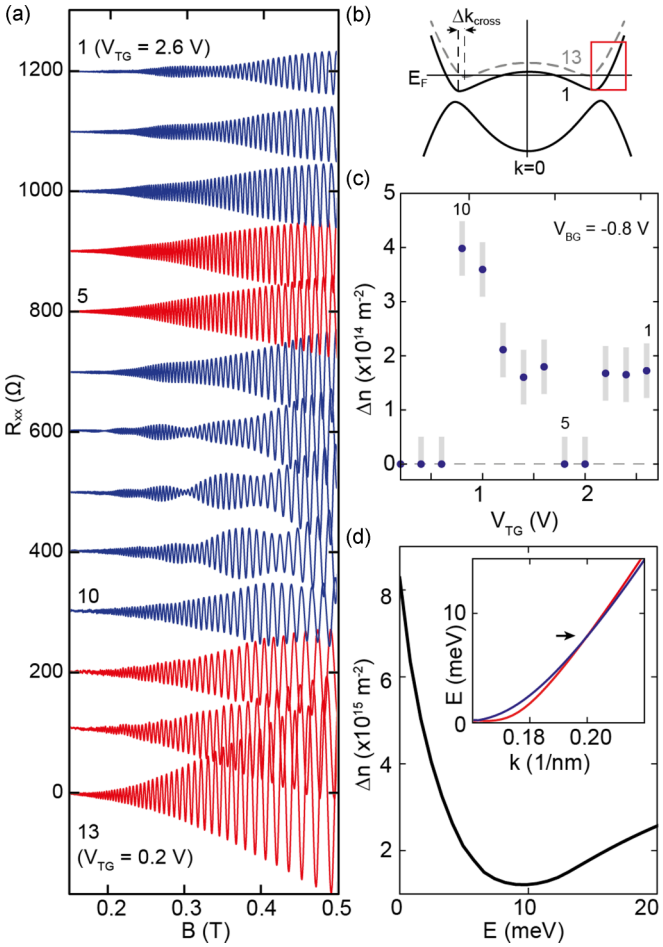

FIG. 4. Spin splitting in the two-carrier regime. (a) Magnetoresistance traces for points 1–13 along line II indicated in Fig. 1. For each trace the $R_{xx}(B = 0)$ background resistance is subtracted and afterwards the traces are offset by 100 Ω. Beating is (not) observed for (red) blue colored traces. (b) Schematic band structure tuning when moving from point 1 to 13. (c) Δn_{ZF} extracted from the Fourier transform of magnetoresistance traces of (a). Error bars are indicated by the light blue bar. (d) Δn_{ZF} extracted from band-structure calculations for our InAs/GaSb quantum well at zero electric field. The inset shows the corresponding band structure in the [100] direction.

respectively. For traces 1–3, at large electron density, beating is observed from which we extract $\Delta n_{ZF} = 1.7 \times 10^{14}$ m^{-2} [35]. Remarkably, traces 4 and 5 do not show any beating, therefore no zero-field density difference can be extracted. For traces 6–10, the beating revives, showing strong beating. Finally, traces 11–13 show no beating. Figure 4(c) depicts the extracted Δn_{ZF} along line II, which shows a nonmonotonic behavior as a function of gate voltage along line II.

In order to understand this nonmonotonic Δn_{ZF} near the hybridization gap (points 1–10) we performed band-structure calculations of our InAs/GaSb quantum well [21]. The Δn extracted from these calculations is plotted in Fig. 4(d), which qualitatively agree with the observed dip in Δn_{ZF} at points 4 and 5 [Fig. 4(c)]. In order to understand the simulated Δn, the band structure near the hybridization gap is depicted in the inset of Fig. 4(d) [the zoom-in on Fig. 4(b) is indicated by the red box]. The blue and red lines represent different spin bands. The bands cross at the black arrow, indicating the vanishing of Δn, such as observed in the experiment. We found this feature to be robust for different electric fields and crystal directions [21]. Interestingly, the crossing of spin bands implies a sign change in SOI strength. Opposite signs of SOI can thus be reached by adjusting the chemical potential. Usually, electric fields are applied to reach such a sign change [36].

Note that only a qualitative comparison between experiment and calculations is possible as only the Fermi energy is varied in the simulation, while in the experiment the band structure (k_{cross}) and Fermi energy are expected to change. The fact that Δn_{ZF} in Fig. 4(d) does not completely vanish is because the crossing of the spin bands in the [110] occurs at a slightly different energy than in the [100] direction.

The lack of beating of traces 11–13 is not captured with the simulation. There are two possible reasons for this deviation. First, a strong asymmetry in the SdH amplitudes of the two spin species ($A_{up} \gg A_{down}$) determines the visibility of the beating pattern. The single spin band SdH oscillation amplitude depends on effective mass m^* and scattering time according to $A_{SdH} \sim (eB/m^*)^3 \exp(-\pi/\omega_c\tau)$ [37]. Both the effective mass and scattering time for the two spin bands become very dissimilar when approaching the hybridization gap [21], as a result that the beating visibility is reduced to below the experimentally detectable visibility. Second, Nichele *et al.* [17] show there is an energy window with only one single spin band present. In such a spin-polarized state no beating can occur. Here, we cannot discriminate between these two reasons that explain the lack of beating in traces 11–13.

In conclusion, we presented a study of the spin-orbit interaction in an InAs/GaSb double quantum well. The Fermi level and band structure are altered by top and bottom gates. In the electron-only regime we find an electric field tunable spin-orbit interaction, and extract the individual Rashba and Dresselhaus terms. In the two-carrier regime we observe a nonmonotonic behavior of the spin splitting which we trace back to the crossing of the spin bands due to the hybridization of electrons and holes.

We gratefully acknowledge Roland Winkler for very helpful discussions. This work has been supported by funding from the Netherlands Foundation for Fundamental Research on Matter (FOM) and Microsoft Corporation Station Q.

[1] R. Winkler, *Spin-Orbit Coupling Effects in Two-Dimensional Electron and Hole Systems* (Springer, Berlin, 2003).

[2] J. Fabian, A. Matos-Abiague, C. Ertler, P. Stano, and I. Žutić, Acta Phys. Slovaca **57**, 565 (2007).

[3] J. Nitta, T. Akazaki, H. Takayanagi, and T. Enoki, Phys. Rev. Lett. **78**, 1335 (1997).

[4] D. Grundler, Phys. Rev. Lett. **84**, 6074 (2000).

[5] B. Shojaei, P. J. J. O'Malley, J. Shabani, P. Roushan, B. D. Schultz, R. M. Lutchyn, C. Nayak, J. M. Martinis, and C. J. Palmstrøm, Phys. Rev. B **93**, 075302 (2016).

[6] I. Žutić, J. Fabian, and S. D. Sarma, Rev. Mod. Phys. **76**, 323 (2004).

[7] S. Datta and B. Das, Appl. Phys. Lett. **56**, 665 (1990).
[8] J. Alicea, Rep. Prog. Phys. **75**, 076501 (2012).
[9] H. Kroemer, Physica E **20**, 196 (2004).
[10] C. Liu, T. L. Hughes, X.-L. Qi, K. Wang, and S.-C. Zhang, Phys. Rev. Lett. **100**, 236601 (2008).
[11] F. Qu, A. J. A. Beukman, S. Nadj-Perge, M. Wimmer, B.-M. Nguyen, W. Yi, J. Thorp, M. Sokolich, A. A. Kiselev, M. J. Manfra, C. M. Marcus, and L. P. Kouwenhoven, Phys. Rev. Lett. **115**, 036803 (2015).
[12] E. A. de Andrada e Silva, G. C. La Rocca, and F. Bassani, Phys. Rev. B **50**, 8523 (1994).
[13] L. J. Cooper, N. K. Patel, V. Drouot, E. H. Linfield, D. A. Ritchie, and M. Pepper, Phys. Rev. B **57**, 11915 (1998).
[14] A. Zakharova, S. T. Yen, and K. A. Chao, Phys. Rev. B **64**, 235332 (2001).
[15] E. Halvorsen, Y. Galperin, and K. A. Chao, Phys. Rev. B **61**, 16743 (2000).
[16] W. Xu, L. L. Li, H. M. Dong, G. Gumbs, and P. A. Folkes, J. Appl. Phys. **108**, 053709 (2010).
[17] F. Nichele, M. Kjaergaard, H. J. Suominen, R. Skolasinski, M. Wimmer, B.-M. Nguyen, A. A. Kiselev, W. Yi, M. Sokolich, M. J. Manfra, F. Qu, A. J. A. Beukman, L. P. Kouwenhoven, and C. M. Marcus, Phys. Rev. Lett. **118**, 016801 (2017).
[18] J. Li, K. Chang, G. Q. Hai, and K. S. Chan, Appl. Phys. Lett. **92**, 152107 (2008).
[19] B.-M. Nguyen, W. Yi, R. Noah, J. Thorp, and M. Sokolich, Appl. Phys. Lett. **106**, 032107 (2015).
[20] L. Onsager, London, Edinburgh Dublin Philos. Mag. J. Sci. **43**, 1006 (1952).
[21] See Supplemental Material at http://link.aps.org/supplemental/10.1103/PhysRevB.96.241401 for the methods regarding Fourier transform and Landau level simulations, and supporting data.
[22] T. H. Sander, S. N. Holmes, J. J. Harris, D. K. Maude, and J. C. Portal, Phys. Rev. B **58**, 13856 (1998).
[23] A. C. H. Rowe, J. Nehls, R. A. Stradling, and R. S. Ferguson, Phys. Rev. B **63**, 201307 (2001).
[24] D. C. Tsui, T. Englert, A. Y. Cho, and A. C. Gossard, Phys. Rev. Lett. **44**, 341 (1980).
[25] V. Gurevich and Y. A. Firsov, Sov. Phys. JETP **13**, 137 (1961).
[26] N. Averkiev, M. Glazov, and S. Tarasenko, Solid State Commun. **133**, 543 (2005).
[27] D. M. Symons, M. Lakrimi, R. J. Nicholas, D. K. Maude, J. C. Portal, N. J. Mason, and P. J. Walker, Phys. Rev. B **58**, 7292 (1998).
[28] D. Shoenberg, *Magnetic Oscillations in Metals* (Cambridge University Press, Cambridge, UK, 1984).
[29] S. D. Ganichev, V. V. Bel'kov, L. E. Golub, E. L. Ivchenko, P. Schneider, S. Giglberger, J. Eroms, J. D. Boeck, G. Borghs, W. Wegscheider, D. Weiss, and W. Prettl, Phys. Rev. Lett. **92**, 256601 (2004).
[30] X. Mu, G. Sullivan, and R.-R. Du, Appl. Phys. Lett. **108**, 012101 (2016).
[31] Note that this g-factor value of -11.5 is measured on a slightly different stack with an InAs layer of 11.0 nm thickness. We have checked in the simulations that changing the g-factor to -5 or -15 has a negligible influence on the SdH oscillations.
[32] F. Herzog, H. Hardtdegen, Th. Schaepers, D. Grundler, and M. A. Wilde, New J. Phys. **19**, 103012 (2017).
[33] Y. A. Bychkov and E. I. Rashba, J. Phys. C **17**, 6039 (1984).
[34] Y. A. Bychkov and E. Rashba, Pis'ma Zh. Eksp. Teor. Fiz. **39**, 66 (1984) [JETP Lett. **39**, 78 (1984)].
[35] We cannot directly extract the spin-orbit strength from this Δn by comparing to the single-carrier case, since the effective mass in this region is unknown.
[36] M. Studer, G. Salis, K. Ensslin, D. C. Driscoll, and A. C. Gossard, Phys. Rev. Lett. **103**, 027201 (2009).
[37] J. Luo, H. Munekata, F. F. Fang, and P. J. Stiles, Phys. Rev. B **41**, 7685 (1990).